Research Article Vol. 30, No. 20 / 26 Sep 2022 / Optics Express 35999
Optics EXPRESS

Beam combining of a broadly and continuously tunable quantum cascade laser

FANGYUAN SUN,[1,4] JINGHAO LI,[1,4] KIAN HUA TAN,[2] SATRIO WICAKSONO,[2] YUN DA CHUA,[1] CHONGWU WANG,[1] MINGJIN DAI,[1] VOO QIN GUI ROTH,[1] SOON FATT YOON,[2] AND QI JIE WANG[1,3,*]

[1]School of Electrical and Electronic Engineering, Nanyang Technological University, Singapore 639798, Singapore
[2]Department of Electrical and Computer Engineering, National University of Singapore, Singapore 117583, Singapore
[3]Centre for Disruptive Photonic Technologies, Division of Physics and Applied Physics, School of Physical and Mathematical Sciences, Nanyang Technological University, Singapore
[4]Equal contributors.
*qjwang@ntu.edu.sg

Abstract: We report a cost-efficient method to demonstrate the beam combining of five laser elements in an array of tunable slot waveguide quantum cascade lasers in the mid-infrared region at around 10 µm. An aspherical lens with five fine-tuned mini mirrors was employed to collimate the individual beams from the laser array. To verify the feasibility of this beam combining approach, the combined beams were coupled into a hollow-core fiber gas cell with a low numerical aperture (N.A.) of 0.03 and a coupling efficiency >= 0.82, for gas sensing of binary compound gases of ammonia and ethylene simultaneously.

1. Introduction

Quantum cascade lasers (QCLs) emitting in the mid-infrared (Mid-IR) range (3~16 µm) have attracted widespread attention [1–4]. Compared to the traditional Mid-IR lasers such as CO_2 lasers and optical parametric oscillators (OPOs), QCLs offer a coherent source with compact size and broad spectral coverage across the whole Mid-IR region [5]. The narrow linewidth, excellent beam quality, broadband tunability and fingerprint absorption for gas molecules render QCL an indispensable tool in spectroscopy applications [6,7], including detection of explosives [8–11], medical diagnostics [12–14], industrial process control [15,16], and environmental monitoring [17–19].

For multi-gas sensing, QCLs with a broad continuous single-mode tuning range are in great demand. Many works on the spectroscopic applications using external cavity (EC) QCLs have been reported due to their mode-hop free tunability over a large wavelength range [20–23]. Nonetheless, EC QCLs relying on mechanically movable gratings hold issues of stability and tuning speed. DFB QCLs tuned by ambient temperature have also been used as the source for spectroscopy [24,25] while the limited tuning range could not fulfill the requirement of scanning the absorption features in a broad spectral range. One significant approach to extend the tuning range of monolithic device is to integrate an array of tunable QCLs lasing at different frequencies monolithically on the same chip. There have been a variety of tunable QCL arrays investigated. The arrays of distributed-feedback (DFB) QCLs [26], master-oscillator power-amplifier (MOPA) QCLs [27], sampled grating distributed-feedback (SG-DFB) QCLs [28,29], and slot waveguide QCLs [30] all demonstrated wide tunability and high Side Mode Suppression Ratios (SMSRs). Nevertheless, the beams of the individual lasers directly from an array could not well overlap in the far-field [31]. Therefore, an effective beam combination is required to implement the tunable

#470631 https://doi.org/10.1364/OE.470631
Journal © 2022 Received 15 Jul 2022; revised 3 Sep 2022; accepted 6 Sep 2022; published 16 Sep 2022

Optics EXPRESS

QCL array devices in the practical sensing application. Wavelength beam combining (WBC) has been demonstrated in both Mid-IR and Terahertz QCLs [31–36]. This method utilizes diffraction gratings to ensure the colinear propagation of the beams from the emitters in the array [37]. For single-mode QCL arrays, the wavelength of all the lasers should be designed to match the dispersion equation of the grating [31–33]. Tuning the emission wavelength of an individual laser of the array will lead to a deviation of beam propagation, which limits the employment of WBC for continuously tunable laser arrays such as SG-DFB QCL arrays and slot waveguide QCL arrays because each individual laser covers a wide tuning range due to the Vernier effect mechanism [38–43]. Another scheme to combine beams is fabricating an on-chip beam combiner integrated with the QCL array. An eight-element SG-DFB QCL array with an on-chip beam combiner achieved a collimated laser beam with displacement < 1.6 mrad over a tuning range of 529 cm^{-1} [28]. However, this on-chip beam combiner induces relatively large additional loss and impairs the output power of lasers. The Arrayed Waveguide Grating (AWG) has also been proposed as an integrated beam combiner in the Mid-IR region [44]. Despite successful demonstration with a DFB QCL array in multi-gas sensing [45], the low power transmission of AWG remains an issue and the crosstalk between channels compromises the SMSRs.

In this paper, we propose a new beam combining method for broadly and continuously tunable QCL arrays and demonstrate it in a five-element slot waveguide QCL array for mixed gas sensing. Slot waveguide QCL arrays hold great potential in multi-gas detection because of their broad mod-hop free continuous tunability and easy fabrication process. However, it is difficult to achieve the beam collinear propagation in a slot waveguide QCL array with WBC as discussed above. Herein, the emission from the five QCL facets is firstly collimated after passing through the aspherical collimating lens. Thereafter, five mini mirrors were used to finely tune the individual beam to make them parallel to each other. Consequently, the beams could be directed to a single point at the back focal plane of the focusing lens. Our method eliminates the influence of the emission wavelength change on the beam combining, so that any adjustments of optical setup were not required throughout the entire tuning range. Moreover, we coupled the combined beams into a hollow-core fiber gas cell to perform sensing for ammonia and ethylene gas mixture as a proof-of-principle application.

2. Beam combining mechanism

The diagram of the beam combining setup is illustrated in Fig. 1. An aspherical lens with an effective focal length (EFL) of f_1 was placed in front of the array at the focus point to collimate the individual laser beams. Because of the different spatial emission positions, the laser beams have distinct propagation directions after the collimating lens and would overlap near the back focal plane of the lens. The angle of the beam from an individual laser with respect to the x-axis will obey the equation: $\theta_i = \arctan(id/f_1)$ referring to the inset of Fig. 1, where i (-m, -(m-1), ... 0, ..., m-1, m) is the number of the laser in the array with a pitch of d. The EFL of the collimating lens is much longer than the pitch of the laser array. Therefore, the equation can be approximately written as:

$$\theta_i \approx id \times 180/(\pi f_1) \tag{1}$$

In this case, each of the QCL beams will be separated spatially in the far-field [31]. Then a series of mini mirrors (MMs) will be placed at specific angles to make all the beams parallel to each other so that they could be directed to a point via one focusing lens. We assume the mini mirror MMi has an angle of φ_i to the beam direction of QCL 0, which can be calculated based on the Eq. (1) as:

$$\varphi_i \approx 45^\circ + \theta_i/2 \tag{2}$$

The distance L between the adjacent beams should be designed as small as possible to reduce the entire combined beam size. This could be accomplished by adjusting the center-to-center

Optics EXPRESS

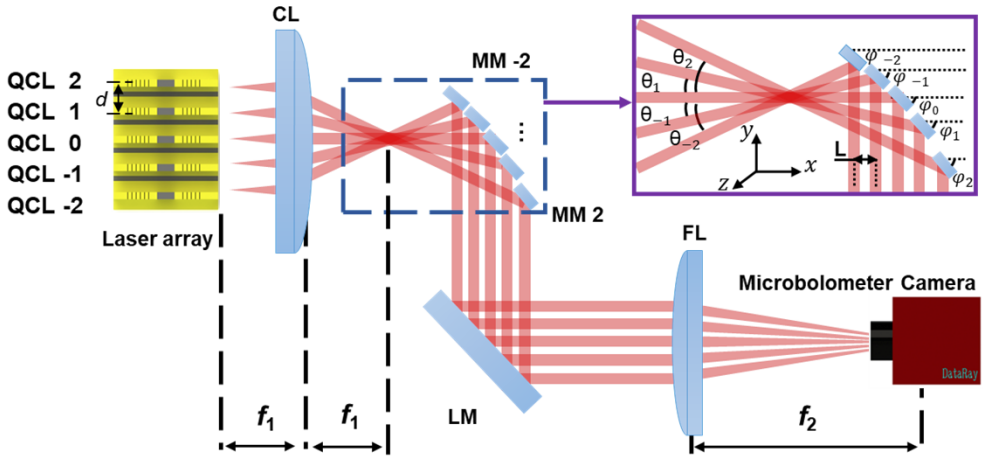

Fig. 1. Schematic diagram of the beam combining from top of view (in x-y plane). Inset: the emitted beam direction and the mini mirror position. MM_i: mini mirror. LM: large mirror. CL: collimating lens. FL: focusing lens. i is the number of the small mirror. f_1 is the focal length of the CL. f_2 is the focal length of the FL. θ_i is the beam direction angle related to the axis of the CL. φ_i is the angle between the mirror and the x-axis. L is the spacing between the adjacent beams. d is the pitch of the laser array.

spacing along the x-axis between adjacent mirrors. Finally, the focusing lens with a focal length of f_2 was employed to overlap the beams in the far-field. The microbolometer camera placed at the back focal plane of this focusing lens was utilized to verify all the beams were focused to a single point. This scheme did not require optical adjustment throughout the entire tuning range because no diffractive optical elements were used.

3. Continuously tunable slot waveguide QCL array

An array of five slot-waveguide QCLs with various emission frequencies were fabricated on a single chip, which was designed based on the same principle proposed in Ref. [30] to realize a broad continuous tuning range free of unexpected mode hoping. A typical bound-to-continuum active region design at around 10 µm is adopted for the growth of the QCL wafer [46]. The device had a similar fabrication process to that in Ref. [30] except that a thicker top gold contact ~ 2 µm was deposited. As Fig. 2(a) illustrates, each laser ridge composed of two electrically separated sections is of the dimension 25 µm × 5.5 mm ×10 µm. The center-to-center distance between two nearby ridges is 300 µm that matches the design of beam combing system. The inset of Fig. 2(a) shows a scanning electron microscope (SEM) image of the fabricated slot QCL array.

The laser array was operated under room temperature. Figure 2(a) also provides the circuit schematic used in this work. For each section of an individual laser, a DC current and a pulsed current (200 ns/5 kHz) combined through the bias-tee were injected.

Different from the previous scheme with only the front section pumped, in this work both sections were pumped by pulsed currents simultaneously. The main purpose of this scheme is to enhance the output powers of single modes. It should be noticed that the two pulsed currents applied on the dual sections must be kept synchronized with the same repetition rate and pulse width, which makes sure the light could be gained at both sections in one cavity roundtrip. A current with a small duty cycle and pulse width (in this work 0.1%, 200 ns) holds a weak ability to tune the refractive index owing to the limited generated and accumulated heat. The spectral tuning behavior of single modes with dual-section pumping is thus the same as the ones of

Optics EXPRESS

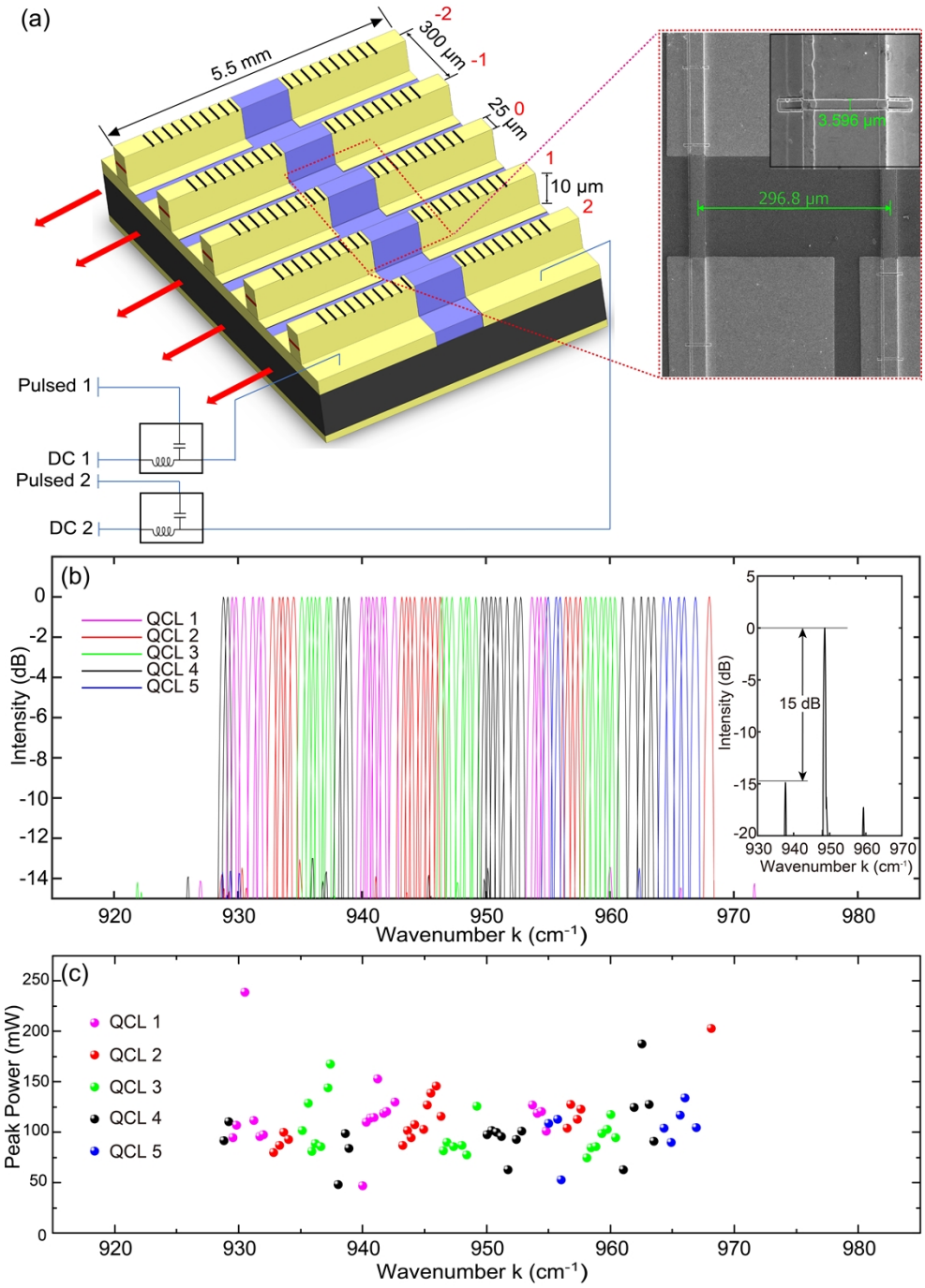

Fig. 2. (a) Schematic diagram of the array based on slot waveguide QCLs. The five lasers are labelled as 2, 1, 0, -1, -2 as per the design of beam combination. A DC current and a pulsed current were combined through the bias-tee into the front (back) section of each laser. The two pulsed currents into the two sections were kept in phase. The inset on the right side is SEM image of the array device showing the ridges and slots. (b) Single-mode tuning spectra of the five-emitter slot waveguide QCL array with an average tuning step ~ 0.4 cm^{-1}, where the modes of different emitters are indicated with different colors. The inset shows one of single-mode spectra at 950 cm^{-1} with a typical SMSR of ~ 15 dB. (c) The peak emission output power of the recorded modes versus the wavenumber.

Optics EXPRESS

previous works using one-section pumping in Ref. [30] and [43] which is mainly controlled by the two DC currents to induce refractive index change by joule heating.

In the practical experiment, we utilized our home-programmed system to keep the two pumping currents synchronized, which were confirmed by a multiple-channel oscilloscope. For convenience, we set the two pulsed currents with the same value. By varying the DC current on the back section from 0 to 1000 mA (with 50 mA step) and supplying proper DC current on the front section from 0 to 1000 mA accordingly, we realized a continuous tuning from 927 to 968 cm^{-1} with an average SMSR of 15 dB. The measured single-mode tuning spectra of the five lasers by a Fourier Transform infrared spectroscopy (FTIR) system with a resolution of 0.2 cm^{-1} are plotted in Fig. 2(b). The value of pulsed current was also adjusted to get the highest power for each single mode frequency. Eventually we achieved single-mode operations with peak power >=49 mW throughout the entire demonstrated continuous tuning range as shown in Fig. 2(c). The dual section pumping scheme significantly increased the powers of single modes without degrading the SMSRs compared to the previous study of Ref. [30], which contributes to signals with a higher signal-noise ratio in practical gas sensing. The frequencies of the single modes in Fig. 2(b) and their corresponding currents were recorded for the demonstration of beam combination and gas sensing.

4. Experimental demonstration and results

The experimental demonstration of the beam combination was based on the setup presented in Fig. 1. To keep a low propagation loss, all the lenses in the setup have an anti-reflection coating (< 2%) from 8 to 12 µm, and the reflective mirrors coated by high-quality gold have a large reflectance (> 98%) in the Mid-IR range. The five-emitter slot waveguide QCL array as described above was chosen as the source. An aspherical lens with an EFL of 6.35 mm (model no. 39504, Edmund Optics Inc.) was utilized as the CL in Fig. 1 to collimate all the laser beams from the array, and the consequent beam patterns of the five QCLs were characterized by a microbolometer-based camera (WinCamD-IR-BB, DataRay Inc.). Figure 3 illustrates the beam patterns of the five lasers under a single longitudinal mode operation in y-z plane corresponding to Fig. 1. Remarkably, the y and z axes represent the horizontal and vertical direction of the beam patterns respectively. It can be observed that the beam pattern of QCL 0 has a dimension of 3.3×7.9 mm defined by $1/e^2$ fullwidth, which illustrates the excellent collimation. As the QCLs were equally spaced, the position of all the QCLs except QCL 0 would be off-axis relative to the collimating lens. In this case, the collimated beams from these off-axis QCLs will be affected by coma aberration [47] as shown in Fig. 3, which makes the beam profiles with a "comet-like" shape especially for the lasers placed far from the optics axis (QCL -2 and 2). The beam spot dimensions of QCL -2, -1, 1 and 2 were 1.9 mm × 2.6 mm, 1.7 mm × 4.2 mm, 2.0 mm × 4.3 mm, and 3.1 mm × 2.8 mm respectively measured in $1/e^2$ fullwidth. The QCL 0 demonstrated a maximum beam size of 3.3 mm in the y-axis direction compared to other lasers. To ensure each individual beam could be reflected solely by the corresponding mirror, a center-to-center spacing between adjacent beams was set as 3.3 mm. Referring to Eq. (1), the adjacent beams after the collimating lens were separated with an angle of $|\theta_i - \theta_{i-1}| = 2.705°$, where i (-2, -1, 0, 1, 2 and $-2 \leq i\text{-}1 \leq 2$). A distance of ~ 90 mm from MM 0 to the front facet of the QCL 0 was then calculated by $2f_1 + 3.3\ \text{mm}/\tan(2.705°) + 2 \times 3.3$ mm. The angle of MM 0 relative to the x-axis should be set as 45° according to Eq. (2). A six-axis manual stage (Model No. E2200B, Suruga Seiki Co., Ltd.) with an angular resolution of 0.009° was adopted to finely adjust MMs to the required angles. The positions and angles of other MMs were determined by placing the microbolometer camera at the back focal plane of the focusing lens in Fig. 1 to monitor whether the corresponding beams would be overlapped with that of QCL 0. In this way, the required positions and angles relative to the x-axis ($\varphi_{-2} = 39.586°$, $\varphi_{-1} = 42.293°$, $\varphi_0 = 45°$, $\varphi_1 = 47.707°$, $\varphi_2 = 50.414°$) of the five mini mirrors were obtained. After that, the MMs were secured with a

Optics EXPRESS

UV adhesive at the determined positions and angles. Consequently, all the beams from the array would propagate in parallel after reflection by MMs, which makes it possible to focus the beams to a point at the focal plane with only one lens.

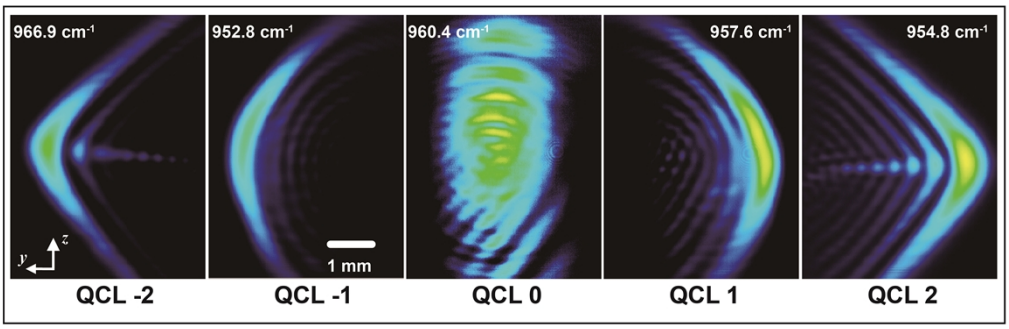

Fig. 3. Beam patterns of the five QCLs in the array after passing through the collimating lens. The patterns from QCL -2 to QCL 2 were recorded under single-mode operation in frequency domain at the wavenumber of 966.9 cm^{-1}, 952.8 cm^{-1}, 960.4 cm^{-1}, 957.6cm^{-1}, and 954.8 cm^{-1} respectively.

Figure 4 depicts the spots of the beams in y-z plane corresponding to Fig. 1 after being focused by the ZnSe plano-convex lens with a focal length of 200 mm as the FL in Fig. 1. The beam spots from QCL -2 to QCL 2 were 1.29 mm × 0.55 mm, 1.32 mm × 0.47 mm, 0.69 mm × 0.42 mm, 1.23 mm × 0.59 mm, and 1.37 mm × 0.52 mm in $1/e^2$ fullwidth measured by the same camera. Owing to the coma aberration in the horizontal direction, the far-field profile of QCL 2 or -2 along the slow axis was twice as wide compared to that of QCL 0. In the vertical direction, the beam spot size exhibits only a slight extension because the coma aberration mainly occurred in the horizontal direction. We also show the beam position relative to the centroid of QCL 0 after focusing lens versus laser number in Fig. 5(a) and 5(b). The peak-to-peak positional error is 0.18 mm along the vertical direction and 0.1 mm along the horizontal direction. The larger positional error in the vertical direction results from the shrinkage and stress generated in this direction during the curing process of UV adhesive when we secured the mini mirrors, which leads to an overall beam spot extension. It is revealed that our approach making use of mini mirrors enables us to realize the overlap of the beams in the far-field. In addition, the efficiency of transferring the optical power from the laser facet to the far-field was around 92%.

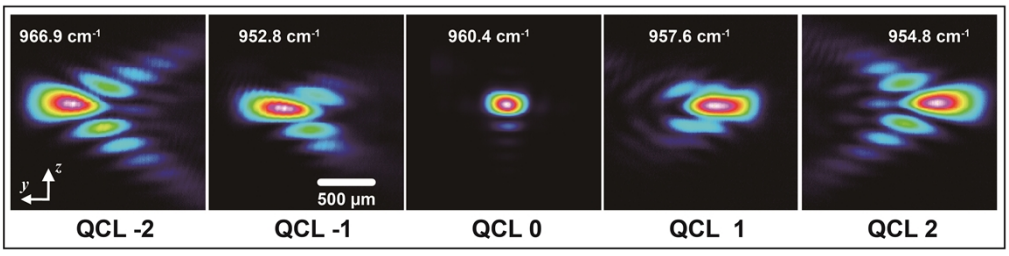

Fig. 4. Beam patterns of the five QCLs in the array at the back focal plane of the focusing lens. The beams from different QCLs were recorded under single-mode operation in the frequency domain at the wavenumber of 966.9 cm^{-1}, 952.8 cm^{-1}, 960.4 cm^{-1}, 957.6cm^{-1}, and 954.8 cm^{-1}.

To demonstrate the effectiveness of this beam combining method, we coupled all the combined beams into a Mid-IR hollow-core fiber with an internal diameter of 1.5 mm and a length of 190

Optics EXPRESS

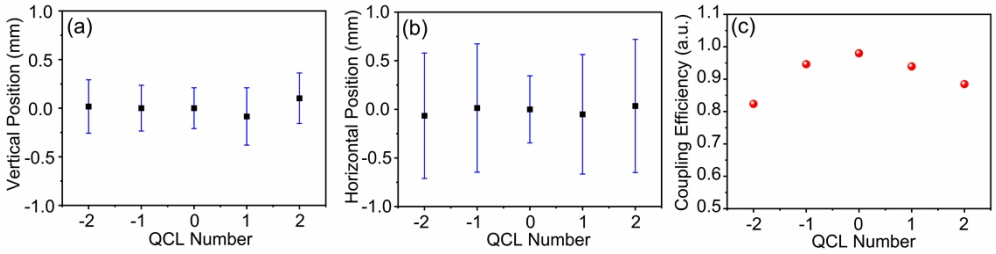

Fig. 5. (a) Beam position along the vertical direction and (b) along the horizontal direction versus QCL number at the back focal plane of the coupling lens. The bar length represents $1/e^2$ fullwidth and the square solid point indicates the centroid of the beam spot. (c) coupling efficiencies of the combined beams from the five QCLs into a Mid-IR hollow-core fiber. For QCL -2, -1, 0, 1 and 2, the coupling efficiencies are 0.82, 0.95, 0.98, 0.94, and 0.88, respectively.

mm. The fiber holds a low N.A. of 0.03 with a good transmission coating at 5-12 μm. The entrance of the hollow core fiber was placed at the back focal plane of the FL in Fig. 1 as a coupling lens. The overall coupling efficiencies considering all five QCLs were measured to be 0.82, 0.95, 0.98, 0.94, and 0.88 respectively as shown in Fig. 5(c). It can be observed that the QCL -1 and QCL 1 have similar coupling efficiencies as for QCL 0, while those for QCL -2 and QCL 2 are slightly lower. Despite the low N.A. of the fiber, high coupling efficiencies larger than 0.8 for all beams were still obtained.

5. Multi-gas sensing demonstration

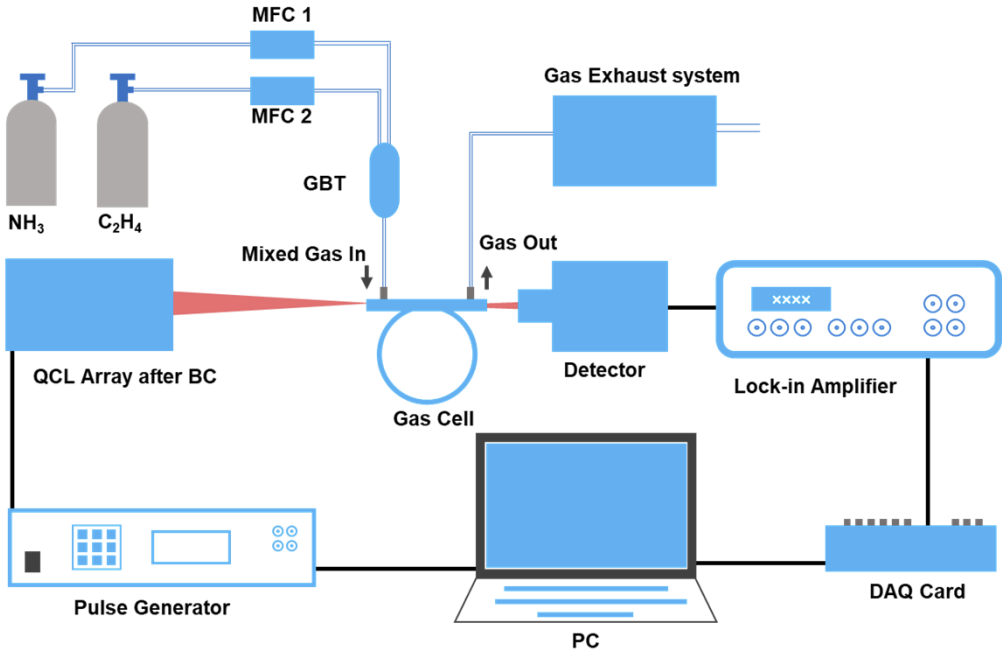

Fig. 6. Schematic diagram of the entire gas sensing setup. QCL array after BC: QCL array after beam combining. DAQ Card: data acquisition card. PC: personal computer. MFC: mass flow controller. GBT: gas blending tube.

Optics EXPRESS

As a proof-of-concept measurement, we performed multi-gas sensing using the same beam combining approach. The entire measurement setup is exhibited in Fig. 6. The combined beams were coupled into a 5 m hollow-core fiber as a gas cell by positioning the entrance of the fiber at the back focal plane of the FL in Fig. 1 with a focal length of 200 mm as a coupling lens. Spectral characterization of the emission passing through the fiber without gas flowing was conducted by FTIR to confirm that the tuning spectra were identical to those in Fig. 2(b). A thermoelectrically cooled Mercury-Cadmium-Telluride (MCT) Mid-IR detector was then placed to collect the laser light through the fiber, from which the signals were demodulated by a lock-in amplifier and recorded with a DAQ card.

Before the sample gas sensing, the fiber cell was filled with pure nitrogen (N_2) at a flowing rate of 200 ml/min as the measurement background. With the same rate flowing through the gas cell, ammonia (NH_3) and ethylene (C_2H_4) were mixed for the demonstration of the simultaneous binary gas detection because they have strong absorptions within the tuning range of our slot waveguide QCL array device. The concentrations of NH_3 and C_2H_4 were both set as 100 ppm. In the practical experiment, each of the analytes was customized at a concentration of 200 ppm where the nitrogen served as the balance gas. As in Fig. 6, The NH_3 and C_2H_4 were respectively controlled by corresponding commercial mass flow controllers (MFCs) to achieve a stable flow rate of 100 ml/min (tolerance < 1 ml/min). Successively, the analytes were filled in a commercial gas blending tube (GBT) where they could be homogeneously mixed and diluted to 100 ppm. Therefore, the combination of MFCs and GBT ensured that the gas mixtures were filled in the gas cell with a stable flow rate of 200 ml/min and each constituent had a constant concentration of 100 ppm. To acquire the absorption spectrum, the single-mode emissions with different frequencies were activated sequentially by applying the calibrated currents to the corresponding lasers and the transmission signals through the gas cell were detected by the MCT detector. This scanning process was automatically controlled by our home-developed LabVIEW program. The data collection time of an individual frequency was set as 5 seconds to stabilize the signal. As a result, it took around 5 minutes to obtain a whole spectrum using the beam combined slot waveguide QCL array. After the scanning of background and sample gases, the absorption spectrum of the sample binary gas mixture could be obtained as presented in Fig. 7, which also provides the individual absorption spectrum of NH_3 (C_2H_4) at 100 ppm from the HITRAN database and the simulated spectrum for the mixture of the two gases. The dominant absorption regions of NH_3 locate at 928 ~935 cm^{-1} and 961 ~969 cm^{-1}, which consist of several extremally sharp absorption peaks. While the absorption peak of the ethylene is centered at 949 cm^{-1} with full width at half maximum (FHWM) ~ 0.5 cm^{-1}. It could be observed in Fig. 7 that the experimental absorption spectrum was in good agreement with the simulated one and the main absorption peaks of the two gases were detected. Our results manifest that the slot waveguide QCL array integrated with this beam combining method has great potential in Mid-IR spectroscopy.

Optics EXPRESS

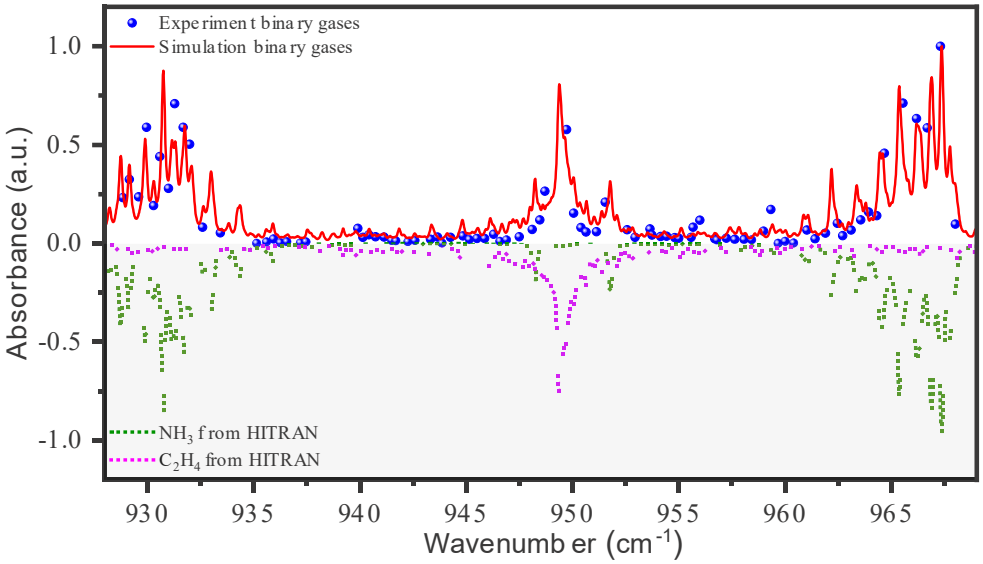

Fig. 7. Absorption spectrum of the gas mixture consisting of 100 ppm ammonia (NH_3) and 100 ppm ethylene (C_2H_4) using the beam combined slot waveguide QCL array represented by blue scatters. The pink and green dash lines respectively show the absorption spectra of NH_3 and C_2H_4 at 100 ppm from the HITRAN database. The simulated absorption spectrum of the binary gas mixture comprised of NH_3 (100 ppm) and C_2H_4 (100 ppm) calculated by *HITRAN on the Web* open access Gas-mixture simulator is displayed in red solid line for comparison with the experimental result.

6. Conclusion

In summary, we achieved beam combining of five lasers from a widely and continuously tunable slot waveguide QCL array by employing an optical configuration consisting of one aspherical lens and five mini mirrors. The efficiency of optical power transmission to the far-field was around 92%. Besides, coupling the combined beams into a hollow-core fiber presented a high efficiency larger than 0.82 for all the beams, which demonstrates the feasibility to apply this beam combining method in practical Mid-IR spectroscopy. This is a compact and cost-efficient beam combining approach that could be employed by different types of QCL arrays. By properly designing the pitch of the lasers in the array and the focal length of the collimating lens, our approach could beam-combine more elements and maintain high coupling efficiency into the fiber for sensing applications. It is convenient to build up a portable system by integrating the beam combined source with gas cells. This work provides a new possible pathway to conducting multi-gas sensing with monolithic broadly continuously tunable QCLs.

Funding. A*STAR grants (A18A7b0058, A2090b0144); National Research Foundation Singapore programme (NRF-CRP18-2017-02, NRF-CRP22-2019-0007)

Disclosures. The authors declare no conflicts of interest

Data availability. The data that support the findings of this study are available from the corresponding author upon reasonable request.

References

1. K. Fujita, S. Furuta, A. Sugiyama, T. Ochiai, A. Ito, T. Dougakiuchi, T. Edamura, and M. Yamanishi, "High-performance quantum cascade lasers with wide electroluminescence (~600 cm^{-1}), operating in continuous-wave above 100 °C," Appl. Phys. Lett. **98**(23), 231102 (2011).

Optics EXPRESS

2. Y. Yao, A. J. Hoffman, and C. F. Gmachl, "Mid-infrared quantum cascade lasers," Nat. Photonics **6**(7), 432–439 (2012).
3. M. Razeghi, W. Zhou, S. Slivken, Q. Lu, D. Wu, and R. McClintock, "Recent progress of quantum cascade laser research from 3 to 12 μm at the Center for Quantum Devices," Appl. Opt. **56**(31), H30–H44 (2017).
4. M. Razeghi, N. Bandyopadhyay, Y. Bai, Q. Lu, and S. Slivken, "Recent advances in mid infrared (3-5 μm) Quantum Cascade Lasers," Opt. Mater. Express **3**(11), 1872–1884 (2013).
5. J. Sun, H. Deng, N. Liu, H. Wang, B. Yu, and J. Li, "Mid-infrared gas absorption sensor based on a broadband external cavity quantum cascade laser," Rev. Sci. Instrum. **87**(12), 123101 (2016).
6. Z. Du, S. Zhang, J. Li, N. Gao, and K. Tong, "Mid-Infrared Tunable Laser-Based Broadband Fingerprint Absorption Spectroscopy for Trace Gas Sensing: A Review," Appl. Sci. **9**(2), 338 (2019).
7. R. S. El Shamy, D. Khalil, and M. A. Swillam, "Mid Infrared Optical Gas Sensor Using Plasmonic Mach-Zehnder Interferometer," Sci. Rep. **10**(1), 1293 (2020).
8. B. Hinkov, F. Fuchs, Q. K. Yang, J. M. Kaster, W. Bronner, R. Aidam, K. Köhler, and J. Wagner, "Time-resolved spectral characteristics of external-cavity quantum cascade lasers and their application to stand-off detection of explosives," Appl. Phys. B **100**(2), 253–260 (2010).
9. C. W. Van Neste, L. R. Senesac, and T. Thundat, "Standoff photoacoustic spectroscopy," Appl. Phys. Lett. **92**(23), 234102 (2008).
10. J. D. Suter, B. Bernacki, and M. C. Phillips, "Spectral and angular dependence of mid-infrared diffuse scattering from explosives residues for standoff detection using external cavity quantum cascade lasers," Appl. Phys. B **108**(4), 965–974 (2012).
11. X. Liu, C. W. Van Neste, M. Gupta, Y. Y. Tsui, S. Kim, and T. Thundat, "Standoff reflection–absorption spectra of surface adsorbed explosives measured with pulsed quantum cascade lasers," Sens. Actuators, B **191**, 450–456 (2014).
12. M. Pleiteza, H. von Lilienfeld-Toal, and W. Mäntelea, "Infrared spectroscopic analysis of human interstitial fluid in vitro and in vivo using FT-IR spectroscopy and pulsed quantum cascade lasers (QCL): Establishing a new approach to non invasive glucose measurement," Spectrochim. Acta, Part A **85**(1), 61–65 (2012).
13. R. Ghorbani and F. M. Schmidt, "Real-time breath gas analysis of CO and CO2 using an EC-QCL," Appl. Phys. B **123**(5), 144 (2017).
14. A. Schwaighofer, M. Brandstetter, and B. Lendl, "Quantum cascade lasers (QCLs) in biomedical spectroscopy," Chem. Soc. Rev. **46**(19), 5903–5924 (2017).
15. R. Lewicki, M. Jahjah, Y. Ma, F. Tittel, P. Stefanski, and J. Tarka, "Mid- infrared semiconductor laser based trace gas sensor technologies for environmental monitoring and industrial process control," Proc. SPIE **8631**, 86310W (2013).
16. H. Moser, W. Pölz, J. P. Waclawek, J. Ofner, and B. Lendl, "Implementation of a quantum cascade laser-based gas sensor prototype for sub-ppmv H2S measurements in a petrochemical process gas stream," Anal. Bioanal. Chem. **409**(3), 729–739 (2017).
17. A. A. Kosterev, Y. A. Bakhirkin, and F. K. Tittel, "Ultrasensitive gas detection by quartz-enhanced photoacoustic spectroscopy in the fundamental molecular absorption bands region," Appl. Phys. B **80**(1), 133–138 (2005).
18. P. Patimisco, G. Scamarcio, F. K. Tittel, and V. Spagnolo, "Quartz-Enhanced Photoacoustic Spectroscopy: A Review," Sensors **14**(4), 6165–6206 (2014).
19. A. Zifarelli, G. Menduni, M. Giglio, A. Elefante, A. Sukhinets, A. Sampaolo, P. Patimisco, S. Fangyuan, W. Chongwu, and Q. J. Wang, "Compact and Versatile QEPAS-Based Sensor Box for Simultaneous Detection of Methane and Infrared Absorber Gas Molecules in Ambient Air," Front. Environ. Chem. **3**, 926233 (2022).
20. R. Centeno, D. Marchenko, J. Mandon, S. M. Cristescu, G. Wulterkens, and F. J. M. Harren, "High power, widely tunable, mode-hop free, continuous wave external cavity quantum cascade laser for multi-species trace gas detection," Appl. Phys. Lett. **105**(26), 261907 (2014).
21. G. Wysocki, R. F. Curl, F. K. Tittel, R. Maulini, J. M. Bulliard, and J. Faist, "Widely tunable mode-hop free external cavity quantum cascade laser for high resolution spectroscopic applications," Appl. Phys. B **81**(6), 769–777 (2005).
22. G. Wysocki, R. Lewicki, R. F. Curl, F. K. Tittel, L. Diehl, F. Capasso, M. Troccoli, G. Hofler, D. Bour, S. Corzine, R. Maulini, M. Giovannini, and J. Faist, "Widely tunable mode-hop free external cavity quantum cascade lasers for high resolution spectroscopy and chemical sensing," Appl. Phys. B **92**(3), 305–311 (2008).
23. A. Hugi, R. Terazzi, Y. Bonetti, A. Wittmann, M. Fischer, M. Beck, J. Faist, and E. Gini, "External cavity quantum cascade laser tunable from 7.6 to 11.4 μm," Appl. Phys. Lett. **95**(6), 061103 (2009).
24. F. Xie, C. Caneau, H. P. LeBlanc, N. J. Visovsky, S. Coleman, L. C. Hughes, and C. Zah, "Room Temperature CW Operation of Mid-IR Distributed Feedback Quantum Cascade Lasers for CO_2, N_2O, and NO Gas Sensing," IEEE J. Sel. Top. Quantum Electron. **18**(5), 1605–1612 (2012).
25. L. Tao, K. Sun, M. A. Khan, D. J. Miller, and M. A. Zondlo, "Compact and portable open-path sensor for simultaneous measurements of atmospheric N2O and CO using a quantum cascade laser," Opt. Express **20**(27), 28106–28118 (2012).
26. B. G. Lee, H. A. Zhang, C. Pflugl, L. Diehl, M. A. Belkin, M. Fischer, A. Wittmann, J. Faist, and F. Capasso, "Broadband Distributed-Feedback Quantum Cascade Laser Array Operating From 8.0 to 9.8 μm," IEEE Photonics Technol. Lett. **21**(13), 914–916 (2009).
27. P. Rauter, S. Menzel, A. K. Goyal, B. Gökden, C. A. Wang, A. Sanchez, G. W. Turner, and F. Capasso, "Master-oscillator power-amplifier quantum cascade laser array," Appl. Phys. Lett. **101**(26), 261117 (2012).

Optics EXPRESS

28. W. Zhou, D. Wu, R. McClintock, S. Slivken, and M. Razeghi, "High performance monolithic, broadly tunable mid-infrared quantum cascade lasers," Optica **4**(10), 1228–1231 (2017).
29. N. Coirier, A. Gomez-Patron, and M. Razeghi, "Gas sensing spectroscopy system utilizing a sample grating distributed feedback quantum cascade laser array and type II superlattice detector," Proc. SPIE **11288**, 1128815 (2020).
30. J. Li, F. Sun, Y. Jin, Y. D. Chua, K. H. Tan, S. Wicaksono, C. Sirtori, S. F. Yoon, and Q. J. Wang, "Widely tunable single-mode slot waveguide quantum cascade laser array," Opt. Express **30**(1), 629–640 (2022).
31. B. G. Lee, J. Kansky, A. K. Goyal, C. Pflügl, L. Diehl, M. A. Belkin, A. Sanchez, and F. Capasso, "Beam combining of quantum cascade laser arrays," Opt. Express **17**(18), 16216–16224 (2009).
32. A. K. Goyal, M. Spencer, O. Shatrovoy, B. G. Lee, L. Diehl, C. Pfluegl, A. Sanchez, and F. Capasso, "Dispersion-compensated wavelength beam combining of quantum-cascade-laser arrays," Opt. Express **19**(27), 26725–26732 (2011).
33. J. Chen, Y. Jin, L. Gao, J. L. Reno, and S. Kumar, "Wavelength beam-combining of terahertz quantum-cascade laser arrays," Opt. Lett. **46**(8), 1864–1867 (2021).
34. J. Zhang, H. Peng, J. Wang, J. Zhang, L. Qin, Y. Ning, and L. Wang, "Dense spectral beam combining of quantum cascade lasers by multiplexing a pair of blazed gratings," Opt. Express **30**(2), 966–971 (2022).
35. S. Hugger, R. Aidam, W. Bronner, F. Fuchs, R. Lösch, Q. K. Yang, J. Wagner, E. Romasew, M. Raab, H. Tholl, B. Höfer, and A. L. Matthes, "Power scaling of quantum cascade lasers via multiemitter beam combining," Opt. Eng. **49**(11), 111111 (2010).
36. Z. Gu, J. Zhang, S. Zhai, N. Zhuo, S. Liu, J. Liu, L. Wang, F. Liu, and Z. Wang, "Spectral beam combining of discrete quantum cascade lasers," Opt. Quantum Electron. **53**(10), 584 (2021).
37. F. Sun, S. Shu, G. Hou, L. Wang, J. Zhang, H. Peng, S. Tian, C. Tong, and L. Wang, "Efficiency and threshold characteristics of spectrally beam combined high-power diode lasers," IEEE J. Quantum Electron. **55**(1), 1–7 (2019).
38. T. S. Mansuripur, S. Menzel, R. Blanchard, L. Diehl, C. Pflügl, Y. Huang, J.-H. Ryou, R. D. Dupuis, M. Loncar, and F. Capasso, "Widely tunable mid-infrared quantum cascade lasers using sampled grating reflectors," Opt. Express **20**(21), 23339–23348 (2012).
39. S. Slivken, N. Bandyopadhyay, S. Tsao, S. Nida, Y. Bai, Q. Y. Lu, and M. Razeghi, "Sampled grating, distributed feedback quantum cascade lasers with broad tunability and continuous operation at room temperature," Appl. Phys. Lett. **100**(26), 261112 (2012).
40. Y. Bidaux, A. Bismuto, C. Tardy, R. Terazzi, T. Gresch, S. Blaser, A. Muller, and J. Faist, "Extended and quasi-continuous tuning of quantum cascade lasers using superstructure gratings and integrated heaters," Appl. Phys. Lett. **107**(22), 221108 (2015).
41. S. Kalchmair, R. Blanchard, T. S. Mansuripur, G.-M. de Naurois, C. Pfluegl, M. F. Witinski, L. Diehl, F. Capasso, and M. Loncar, "High tuning stability of sampled grating quantum cascade lasers," Opt. Express **23**(12), 15734–15747 (2015).
42. B. Meng, J. Tao, X. H. Li, Y. Q. Zeng, S. Wu, and Q. J. Wang, "Tunable single-mode slot waveguide quantum cascade lasers," Appl. Phys. Lett. **104**(20), 201106 (2014).
43. B. Meng, Y. Q. Zeng, G. Liang, J. Tao, X. N. Hu, E. Rodriguez, and Q. J. Wang, "Broadly continuously tunable slot waveguide quantum cascade lasers based on a continuum-to-continuum active region design," Appl. Phys. Lett. **107**(11), 111110 (2015).
44. P. Barritault, M. Brun, P. Labeye, J. Hartmann, F. Boulila, M. Carras, and S. Nicoletti, "Design, fabrication and characterization of an AWG at 4.5 µm," Opt. Express **23**(20), 26168–26181 (2015).
45. L. Bizet, R. Vallon, B. Parvitte, M. Brun, G. Maisons, M. Carras, and V. Zeninari, "Multi-gas sensing with quantum cascade laser array in the mid-infrared region," Appl. Phys. B **123**(5), 145 (2017).
46. R. Maulini, M. Beck, J. Faist, and E. Gini, "Broadband tuning of external cavity bound-to-continuum quantum-cascade lasers," Appl. Phys. Lett. **84**(10), 1659–1661 (2004).
47. E. Hecht, *Optics*, (global edition, Pearson Education UK, 2016), Section 6.3.